Numerical Simulation of an F-16A at Angle of Attack

G. W. Huband,* J. S. Shang,† and M. J. Aftosmis‡
Wright Research and Development Center, Wright-Patterson Air Force Base, Ohio 45433

The transonic flowfield around an F-16A fighter configuration at a moderate incidence angle is simulated by solving the Navier-Stokes equations on a single-block grid. The numerical solution matches experimental freestream conditions with a Mach number of 0.85, 16-deg angle of attack, and a characteristic Reynolds number of 12.75 million. MacCormack's explicit algorithm is used in conjunction with a local time step and consecutive mesh refinement procedure to accelerate numerical convergence. The Baldwin-Lomax algebraic model provides turbulent closure. Computed surface pressure distributions and the aircraft lift coefficient compare favorably with wind tunnel data. The drag coefficient in the simulation overpredicts the experimental value by 8%. The analysis of results details the interactions of the strake vortex and the wing root vortex in an upwash flow. This discussion also focuses on the importance of grid topology and surface definition in the computation of flows at high angle of attack.

Nomenclature

C_D = drag coefficient
C_L = lift coefficient
C_p = pressure coefficient, $[2(p - p_\infty)]/\rho_\infty u_\infty^2$
S = circumferential arc length around the fuselage
L = turbulent length scale
y = vertical coordinate
z = spanwise coordinate

Introduction

COMPUTATIONAL fluid dynamics now has the capability to simulate cruising aircraft in steady motion with accuracy comparable to that of experiments.[1-4] Despite the success of these calculations, the necessary computing resource remains prohibitive for routine design applications. However, a more serious technological barrier still exists, and accurate physical modeling of flows at extreme flight conditions remains elusive. Present and future maneuvering aircraft must operate in an unsteady and vortex dominated flight regime. This time-dependent environment is highly nonlinear and cannot be accurately described by sequential static analyses. Numerical simulation of a maneuvering aircraft requires an interdisciplinary computational aerodynamics (ICA) approach, which couples aerodynamics, flight dynamics, flight control, and aeroelasticity. Among the most elusive of the many scientific issues that remain to be resolved is the ability to capture the detailed aerodynamic phenomena around an aircraft at high angle of attack. At the present time, the numerical resolution required to model unsteady vortex dominated flows remains largely unknown. Moreover, the interaction of vortical structures with turbulence requires further investigation. This deficiency stems from a lack of recognition of the importance of vortex interaction in our early basic research into inviscid-viscous interactions.[5-7] A viable approach to overcome this technical barrier may be derived from additional engineering applications, which would provide a broad knowledge base for reassessment.

A wide array of investigations have examined aerodynamic configurations at high angle of attack. Recently, Thomas et al.[8] and Schiff et al.[9] carried out successful studies of the F-18 forebody. This work alleviated the gridding complication that results from the large leading-edge wing extensions (LEX) by using a multiple block grid. At an angle of attack of 30 deg, the predicted primary and secondary separation lines on the F-18 forebody compare reasonably well with flight data.[8,9] This work shows similar surface shear topologies for both laminar and turbulent calculations. The main difference in these distributions lies in the scaling of the separated regions. This single case, however, does not permit any general conclusions to be drawn for a wider range of incidence angles. This is especially true in moderate angle of attack cases where incipient separation may lead to drastic differences between laminar and turbulent simulations.[10,11] In such problems, laminar-turbulent transition may play a more significant role than is generally anticipated.

Another major component of many high-performance aircraft is the delta wing. Often employed as either the basic planform, wing strake, or LEX, the delta wing generates controlled vortical flow at positive incidence and is known to produce intricate aerodynamic phenomena. As angle of attack increases, these phenomena include both asymmetric vortex formation, and eventually vortex breakdown.[7,12,13] Rizzetta et al. have obtained Navier-Stokes solutions of delta wings at angle of attack for Mach numbers of 1.95, 4.0, and 7.0. These cases produced subsonic, sonic, and supersonic flows normal to the swept leading edge.[14] Laminar and turbulent Navier-Stokes solutions were generated for the sonic normal Mach number flow condition. At 10 deg incidence, the laminar and turbulent solutions demonstrated minimal differences with the most pronounced disparity lying in the scaling of the vortical formations.

Solutions of the simplified governing equations have also been obtained for a variety of slender delta wings at various Mach numbers.[7,15,16] In general, these investigations resulted in good agreement with surface pressure data and surface and vortex flow visualization. More recently, Fujii and Schiff simulated vortical flows over a strake-delta wing at high angle of attack by solving the three-dimensional thin-layer Navier-Stokes equations.[17] This work included a remarkable series of vortical flowfield calculations spanning angles of attack from 6 to 40 deg. In this effort, the numerical simulation also replicated the elusive vortex breakdown phenomena. In spite of the uncertain effects of turbulence and numerical resolution, their achievement clearly identifies key features of strong vortex interaction and breakdown. Despite this, the basic

Presented as Paper 90-0100 at the AIAA 28th Aerospace Sciences Meeting, Reno, NV, Jan. 8-11, 1990; received Jan. 31, 1990; revision received May 31, 1990; accepted for publication May 31, 1990.

*Aerospace Engineer. Member AIAA.
†Technical Manager. Associate Fellow AIAA.
‡Computational Aerodynamicist. Member AIAA.

issues of numerical accuracy and the role of turbulence remain uncertain. An independent and complementary investigation is currently underway to determine the accuracy required to resolve such intricate, unsteady, aerodynamic phenomena.[18]

As a bench mark of technology development, numerical solutions of the rather complex F-16A fighter (Fig. 1) were generated by a coordinated effort.[2,3] The first solution was obtained by solving the mass-averaged Navier-Stokes equations in a single-block H-H grid.[2] The other used the thin-layer, Reynolds-averaged Navier-Stokes equations with a zonal grid structure.[3] These path-finding numerical simulations of complete aircraft at cruising conditions successfully achieved accuracy comparable to that of wind tunnel data. The most recent endeavor in this area is due to Vadyak et al.[19] Using the Reynolds-averaged Navier-Stokes equations, they investigated vortical flowfields around a generic fighter with a blended strake/swept wing. These results recorded vortex breakdown in both the numerical and experimental investigations at 21-deg angle of attack. Their numerical results provide some unique insights but cannot be used to draw definitive conclusions for their findings.

The present analysis attempts to add to the existing knowledge base by computing an F-16A configuration at an angle of attack of 16.04 deg using the mass-averaged Navier-Stokes equations. By deliberately choosing a demanding flight condition, this investigation hopes not only to highlight current simulation capabilities but also to identify future research topics.

Overview of Simulation

In the present analysis, the numerical method solved the time-dependent, compressible, three-dimensional, mass-averaged Navier-Stokes equations. In an effort to minimize the number of arithmetic operations per time step, the system of equations was cast in chain-rule conservation form and in generalized coordinates. Following earlier investigations,[1,2] the simulation made use of a fully vectorized computer code based on MacCormack's explicit scheme.[20] The fact that this code has been validated in applications covering a wide range of aerodynamic phenomena enabled us to focus on the physical aspects of the F-16A flowfield. The Baldwin-Lomax turbulence model[21] used in this investigation contained a simple length scale modification at body junctions of the fuselage-wing and the empennage. At such corners the scaling length in the eddy viscosity formulation was derived from the Buleev integral, employing the asymptotic form to ensure a smooth transition of length scales from one intersecting surface to another.[22] With the corner located at $y=0$ and $z=0$ the length scale is

$$L=\frac{2yz}{y+z+\sqrt{y^2+z^2}}$$

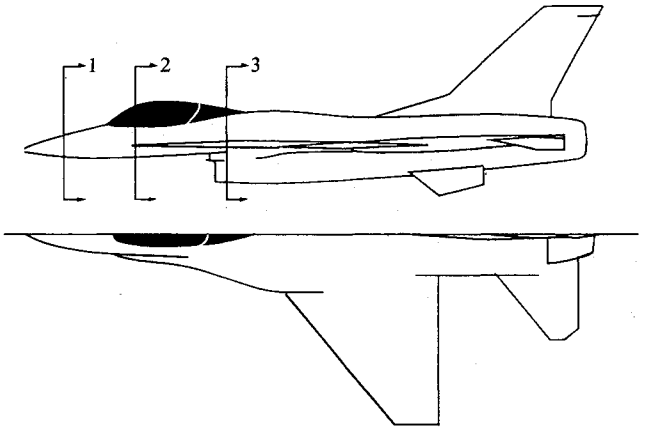

Fig. 1 Geometry of F-16A showing locations of fuselage pressure stations.

The system of equations was formally closed by specifying values of 0.9 for the turbulent Prandtl number by the calorically perfect gas assumption and by Sutherland's law for molecular viscosity.

The F-16A configuration used in the present analysis corresponds to a one-ninth-scale wind tunnel model, which omitted minute details (i.e., antennas). In the present investigation, missile rails, missiles, ventral fin, lip of inlet, and the slots between the fuselage and control surfaces of the empennage were not modeled. Based on an analysis of aerodynamic force data, these simplifications cause no significant degradation to the overall aircraft performance parameters (C_L, C_D). Unfortunately, these alterations could prevent a detailed comparison of data and numerical results at isolated regions of interest. The only improvement to the aircraft surface definition over the earlier study focused on increasing resolution of the wing leading edge. This grid augmentation attempted to better resolve the leading-edge suction of the wing. This suction peak was the only noticeable disparity between data and calculation in the previous investigation.[2] Since the present study made no attempt to simulate flight with sideslip, it only considered a half configuration divided by the plane of symmetry.

The computed flow conditions are defined by a freestream Mach number of 0.85- and 16.04-deg angle of attack and a characteristic Reynolds number, based on aircraft body length, of 12.75 million. The numerical simulation duplicated wind tunnel test conditions of Ref. 23 with an unperturbed freestream temperature of 473.8°R and pressure of 700 psf. The experimental data base includes selected static pressure distributions on the fuselage, wing, and empennage, as well as integrated results for lift and drag coefficients.

The basic H-H grid topology for the F-16A simulation was established by Karman, Steinbrenner, and Kisielewski in their effort to obtain an Euler solution.[24] The complex aircraft geometry compelled the adoption of a zonal grid construction, defining the complete configuration with 20 grid blocks. The majority of these blocks were concentrated around the inlet and the empennage. Individual grid blocks describing specific local features of the configuration were then merged into a single global block. This single global structure completely eliminates artificial zonal boundaries, and their associated numerical errors, from the computation. Unifying the grid blocks in pre-processing also avoids repetitive flux calculations across the artificial internal boundaries. At the zone interfaces, all parametric lines were aligned and smoothed by a Poisson-averaging process so that all coordinates were continuous at least to the first derivative. The same process was also used to cluster and enhance the orthogonality of the grid system adjacent to the body surface.

Boundary Conditions

In the simulated transonic flowfield, the incoming and outgoing flow boundaries were placed at 1.79 and 1.82 aircraft lengths upstream and downstream from the aircraft apex, respectively. In the vertical direction, the computational domain spanned 11.56 wing root chords. In the lateral space, the outer boundary was placed at 5.56 half spans from the plane of symmetry.

The boundary conditions on the aircraft surface were straightforward. The no-slip condition was imposed on all three velocity components. The constant surface temperature of 543°R and the isobaric condition normal to the surface determined the values of density and the internal energy.

On the plane of symmetry, numerical boundary conditions stipulated vanishing gradients and zero velocity component normal to the plane. The latter reflected the fact that the plane of symmetry must coincide with a stream surface.

The propulsion system required the specification of boundary conditions at the engine inlet and nozzle exit. Since the modeling neglected all details of the propulsive system, the simplest possible boundary conditions for the flow-through

arrangement of the wind tunnel test[2,23] were simulated by a no-change approximation at the inlet. At the nozzle exit a parabolic velocity distribution was specified.

The implementation of far-field boundary conditions for transonic flows is constrained by our limited knowledge of the rank and number of negative eigenvalues of the coefficient matrix of the Navier-Stokes equations.[6,25] This difficulty was further compounded by the relatively close placement of the computational domain to the simulated aircraft. Thus, the well-known one-dimensional inviscid approximation should be implemented to minimize any non-physical reflections of disturbances from the boundaries.[26,27] This work stipulates that the boundary conditions will be over specified if all velocity components, density, and pressure are given simultaneously. In the present analysis, the velocity and the density were prescribed by the unperturbed freestream value and the pressure was allowed to adjust itself according to the local conditions. The alleviation of spuriously reflecting wave systems within the computational space was almost immediate. This observation ensured that the imposed far-field boundary conditions were well posed and physically meaningful.

Numerical Procedure

The entire flowfield around the F-16A configuration was solved on two grid systems. The coarse initial grid consisted of 82 × 57 × 41 nodes in streamwise, vertical, and spanwise directions, respectively. The sole purpose of the coarse-grid computation was to provide a good initial condition for the calculation on the finer mesh. For the coarse-grid solution, the convergence criteria was not enforced. Past experience dictates that the numerical resolution of the coarse-grid result is insufficient to provide reliable engineering data.[1,2] Therefore, information for the dependence of solution accuracy on grid density was not recorded. The actual numerical simulation was processed on a mesh containing just over 1.4 million nodes. In the streamwise direction, 158 grid planes were used from the apex of the F-16A to the outflow boundary with 135 nodes on the fuselage of the aircraft. However, the total number of nodes between boundary surfaces in the streamwise direction was 199. The additional 41 points resulted from a coordinate rotation, which places outboard nodes farther upstream of the nose. Reference 2 gives a more detailed description of the basic grid topology. A total of 112 planes describe the vertical direction of the domain using 53 and 59 coordinate surfaces in the leeward and windward space, respectively. Outward along the span, 81 points were used between the plane of symmetry and the outer boundary surface. The upper and the lower fuselage surfaces were defined by 41 spanwise nodes. In spite of the seemingly large number of the grid points used, the local grid density remained relatively sparse in some locations. For example, the entire wing was resolved with 37 streamwise stations and the half span contained only 21 planes. This is certainly quite coarse in comparison with typical grid densities over wings.[6]

In the present analysis, the viscous-dominated region included roughly 325,000 nodes, or about 23% of the total grid points. The grid spacing normal to body surface maintained a value of y^+ of between 2 and 3 near the trailing edge of the wing. A uniform step size immediately adjacent to the body was not enforceable, but even the forebody and wing leading edge maintained a y^+ value of less than 10. Since the present investigation sought only the steady-state asymptote, numerical convergence was accelerated by means of a local time step scheme. This procedure was used exclusively after a short initial transient phase of evolution.

The data processing rate for the coarse-mesh and the fine-mesh calculation achieved 3.06 and 3.38×10^{-5} s per iteration per grid point, respectively, on a single processor of a Cray 2 computer. The CPU time required to sweep the entire flowfield for the fine-mesh computation was 48.5 s. For a complex flowfield containing separated flow regions, vortices, jet stream and wake, a single criterion for numerical convergence is inadequate. This observation led to the monitoring of both global and local flow quantities. The primary numerical convergence criterion watched the evolution of the lift coefficient, and the solution was considered to have reached a steady state when the lift coefficient changed less than one-tenth of 1% after 1000 iterations. To ensure that the final solution had indeed reached its steady asymptote, selected pressure distributions and shear-layer velocity profiles on the wing surface were also monitored.

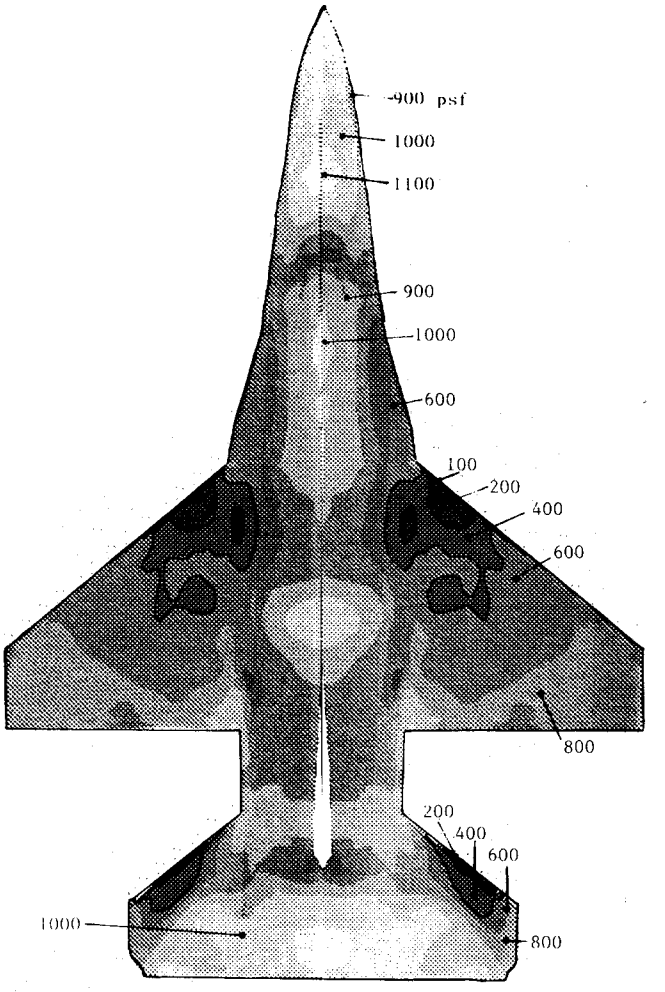

Fig. 2 Computed pressure distribution on F-16A at Mach 0.85 and 16.04-deg angle of attack.

On the coarse grid, 19,000 iterations were performed for a total of 31 single processor CPU h (the code was run on one CPU). On the fine grid, 21,000 iterations were performed for a total of 254 single processor CPU h. Out of this total, approximately 10 h were used for trial and error resulting in 275 total CPU h for the project. Estimated time for an implicit code to solve the same problem is between 80 and 100 CPU h.

Discussion of Results

The numerical results are presented in three major sections. After first comparing computed results with detailed pressure measurements at a variety of locations, focus shifts to a discussion of the global aerodynamic parameters. Then, after establishing the accuracy of the simulation, the discussion highlights some physical features of the flowfield.

Specific Comparison with Data

Figure 2 depicts the computed pressure contours on the leeward surface of the F-16A. This figure serves not only as an illustration of the general features of the numerical simulation but also as an outline for subsequent detailed compari-

sons. Downstream of the aircraft apex, the expansion around the forebody and the ensuing compression to align the flow with the plane of symmetry creates a nearly isobaric leeward surface. The vortex-induced pressure trough[14,18] expected at the leading edge of the strake cannot be identified in either the experiment or the calculation. However, both the streamwise compression and expansion of flow as it negotiates the canopy are easily detectable. As expected, the most severe pressure variations appear on the wing and the horizontal tail surface. The upwash induced rapid expansions concentrate along the leading edge of these lifting surfaces. Downstream of the leading edges, the pressure level on both surfaces increases, either by an embedded shock wave system or by a gradual compression process, toward the trailing edges.

The aerodynamic interference of lifting surfaces and fuselage exerts a strong influence on the pressure distributions in the region of wing-body and empennage junctions. The pressure contours also exhibit a strong outboard tip effect. Intricate aerodynamic phenomena like these are too complex to be described by the pressure field alone.

The circumferential surface pressure distribution at 0.13 aircraft length from the apex is presented in Fig. 3 (station 1 in Fig. 1). The ordinate of the graph represents the normalized arc length tracing the cross section of the fuselage. This

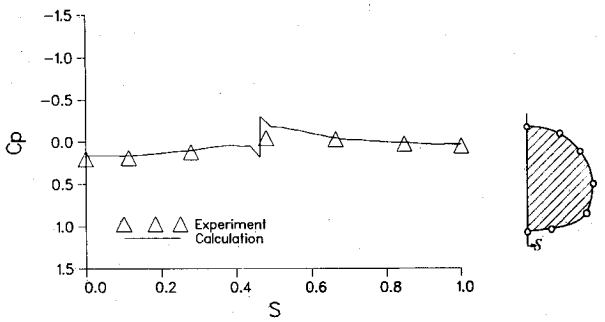

Fig. 3 Comparison of computed pressure distribution with that of Ref. 23 at fuselage station 1.

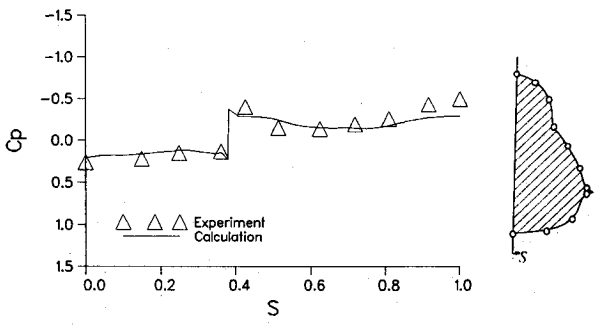

Fig. 4 Comparison of computed pressure distribution with that of Ref. 23 at fuselage station 2.

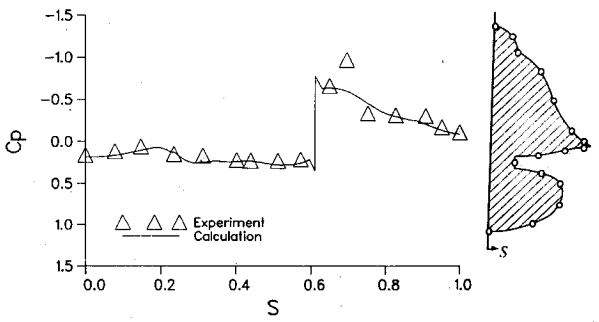

Fig. 5 Comparison of computed pressure distribution with that of Ref. 23 at fuselage station 3.

distance is measured from the windward to leeward plane of symmetry. Since no grid surface intersects the fuselage at the data collecting station, results were linearly interpolated from adjacent gridlines to the location of the pressure taps. The agreement between data and calculation is excellent, and the only disparity appears at the midpoint of the fuselage cross section. To insure smoothly varying metrics near the aircraft surface, some smoothing of the body was necessary. In areas where the top and bottom of the body meet, this smoothing resulted in a very small chine, which causes the oscillation at approximately $S = 0.45$. Nevertheless, the numerical result accurately predicts the pressure difference at the symmetry plane.

In Fig. 4, the pressure coefficient of the forebody at a distance of 0.23 aircraft length from the apex is given (station 2 in Fig. 1). At this streamwise location, the canopy and the forebody strake begin to emerge from the fuselage. Here, the flowfield undergoes a rapid adjustment as it compresses at the front of the canopy. At this station the simulation predicts the peripheral pressure jump across the sharp strake to within the scatter band of the test data.

Figure 5 depicts the pressure coefficient over the most complex cross section of the aircraft. This plane contains the trailing portion of the canopy, the strake, and the diverter connecting the fuselage and propulsion duct (see the sketch of station 3 inset with the plot). The measurements and the numerical results compare very well with the maximum deviation remaining below 5%. The numerical result predicts correctly the expansion from the windward plane to the mid-section of the duct and a compression ahead of the domain bounded by the duct, the diverter and the strake. Within the confined domain ($0.3 < S < 0.6$) just beneath the strake, the pressure distribution is nearly constant. Following the surface coordinates S a rapid expansion of flow around the leading edge of strake yields a huge pressure difference across the leeward and the windward surfaces. On the leeward surface, a continuous compression process extends from the tip of the strake to the top of the canopy. The pressure coefficient distribution indicates that the fuselage/strake combination will make a significant contribution to overall aircraft lift.

Figure 6 represents the wing root pressure distribution along the chord. At a positive angle of attack, the wing root is completely immersed within the strake vortex and a complex inviscid-viscous interaction takes place. Such complex physical features make any shortcoming of numerical simulation especially apparent. As expected, the data and the computation disagree most severely over the leeward surface. The largest deviations between the data and calculation occur at the leading edge and the midchord of the wing. The maximum difference is about 17%. In spite of the seemingly random discrepancy between the data and the calculations, two isolated sources produce the lack of accord at the leading and the trailing edges.

At the leading edge, lack of resolution forces the numerical result to overpredict the extent of the separated region making it unable to capture the leading-edge suction peak. In a tran-

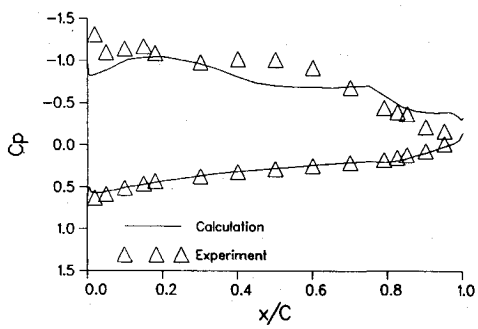

Fig. 6 Comparison of computed wing root pressure distribution with that of Ref. 23.

sonic flow, a slight difference in Mach number distribution about the leading edge may lead to a different mechanism shaping the flow structure downstream. Under close examination, the numerical result follows the trend of data and the physics until seven-tenths chord but over an inaccurate length scale. Most of the numerical errors in this area are induced by the poor prediction of the flow at the leading edge. Efforts to improve the numerical resolution and the leading-edge definition of the wing have been attempted but obviously remain insufficient. The H-H grid structure compounds the resolution problem by inhibiting the grid's ability to correctly describe the nose radii of the leading edge. The influence of the turbulence model on the prediction is much less certain. This modeled turbulent behavior is surely non-physical near the separation bubble on the leading edge.

The disparity between data and calculation at the trailing edge of the wing is incurred by rounding the sharp edges of the fuselage/wing juncture. The upwash over the rounded edges produces a weaker expansion from the trailing edge toward upstream than recorded in the experiment. The windward surface of the wing root is exposed to a relatively undisturbed oncoming stream. The numerical resolution required to describe the physics is much less demanding than in the leeward region. Therefore, the pressure coefficient over the windward surface remains in nearly perfect agreement with the data.

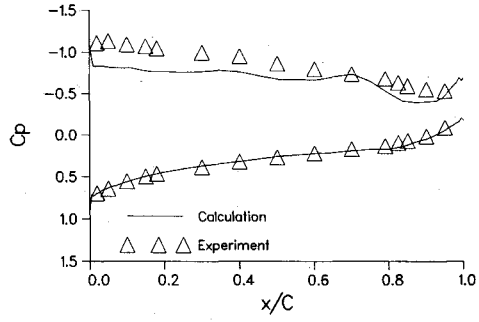

Fig. 7 Comparison of computed pressure distribution with that of Ref. 23 at six-tenths span on the main wing.

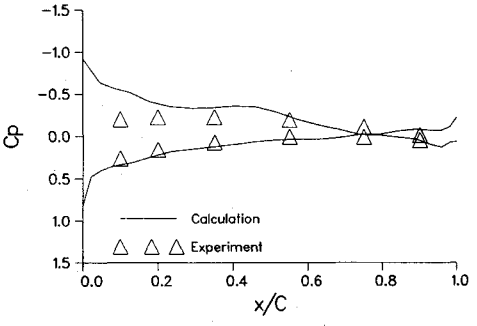

Fig. 8 Comparison of computed pressure distibution over the horizontal stabilizer with that of Ref. 23 at one-third span.

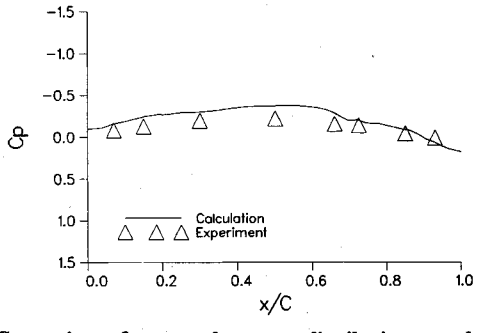

Fig. 9 Comparison of computed pressure distribution over the vertical stabilizer with that of Ref. 23 at half span.

Table 1 Comparison of aerodynamic force coefficients with data of Ref. 23

	Data	Calculation	Discrepancy, %
C_L	1.190	1.188	−0.2
C_D	0.324	0.352	+8.6

Figure 7 describes the pressure coefficients on the wing at six-tenths span. Again, the numerical result overpredicts the leeward surface pressure, and the difference between results diminishes as the flow proceeds downstream. At the leeward trailing region, numerical results follow the trend of data but exhibit a more pronounced variation due to the local expansion. The maximum deviation between data and calculation again occurs at the leading edge with a magnitude of less than 16%. The source of this numerical deficiency is clearly displayed by the overcompression at the leading edge. In this region, the flow expands over the leading edge and undergoes a compression in an extremely short distance. This large disturbance could initiate boundary layer transition, which is beyond our current capability to model with confidence. However, this observed discrepancy is still believed to be induced by the deficiency in numerical definition of the leading edge. The excellent agreement of the windward pressure distribution with data supports this assertion. Since the stagnation point is located downstream of the leading edge and on the windward surface, only a monotonic expansion persists from leading to trailing edge. The numerical result correctly duplicates the measured pressure distribution on the windward surface of the wing.

Figure 8 compares surface pressure from the experiment and calculation on the horizontal stabilizer at one-third span. The basic flow structure is similar to that of the wing and the general behavior of numerical solutions should likewise be analogous. Given this, one might expect perfect agreement between the data and the numerical results on the windward surface, and a maximum deviation of 14% over the lee side surface. However, the leading-edge compression is now underpredicted and leads to a slightly more vigorous sequence of compression-expansion events starting around midchord and proceeding downstream. Again, the departure from data at the leading edge results from insufficient numerical resolution. The small difference around the midchord is a few percent.

The last surface pressure comparison examines the vertical stabilizer. The data and calculations around half span are depicted in Fig. 9. At this angle of attack with no sideslip, the flow over the vertical stabilizer roughly compares to a swept back wing with no incidence. In spite of the fact that the control surface is partially immersed in the wake of the fuselage and wing, the effects of shear-layer interaction are rather limited. On this control device, the surface pressure varies mildly around the freestream value with deviations of only a few percent.

In summary, comparison of computed pressure with data demonstrate that the numerical results duplicated all primary features of the wind tunnel data. At this moderate angle of attack, nearly all major discrepancies between data and present results emanate from the upwash around leading edges of the lifting surfaces. Several probable sources of numerical errors can be easily identified, but the poor leading-edge definition afforded by the single-block H-H topology is believed to be most critical. In future analyses, the numerical resolution issue must be addressed before any other considerations.

Aerodynamic Coefficients

Table 1 summarizes the integrated aerodynamic parameters C_L and C_D from the measurement[23] and the present numerical simulation. The excellent agreement between data and the computed lift coefficient suggests an internal cancellation of

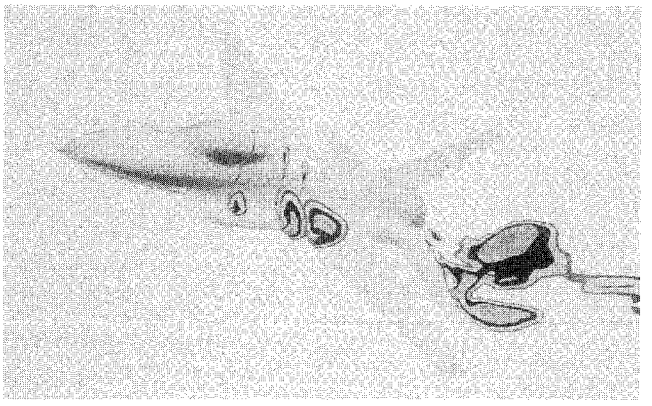

Fig. 10 Pitot pressure contours in selected streamwise planes showing the development of the strake and wing tip vortices.

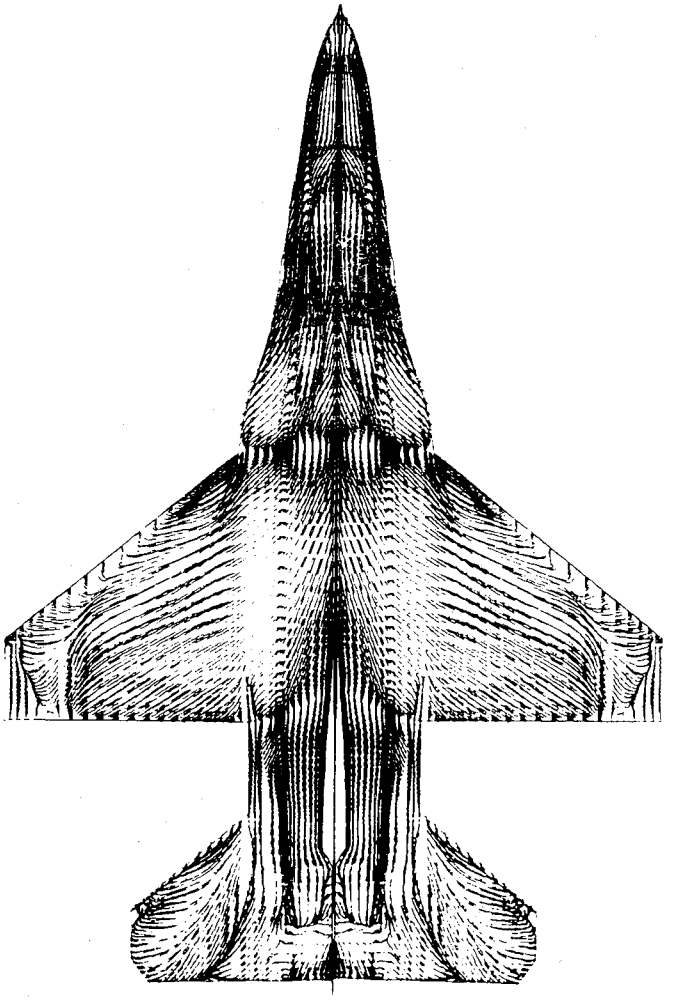

Fig. 11 Simulated oil flow patterns showing surface shear stress distribution.

errors in the surface integration process. Based on the detailed comparison of pressure distributions on lifting surfaces, known discrepancies could lead to a difference of about 7%. As a point of reference, the earlier simulation[2] of the same aircraft at a Mach number of 1.2- and 6-deg angle of attack produced a difference of 5.0 and 5.6% in lift and drag coefficient from data,[23] respectively. One may conclude that the global aerodynamic parameters from the present analysis remain consistently credible. A breakdown of the aerodynamic coefficients showed that the fuselage/strake contributed 54% of the lift and 58% of the drag, whereas the wing contributed 42% of the lift and 38% of the drag. As reference, the earlier supersonic simulation[2] showed that the

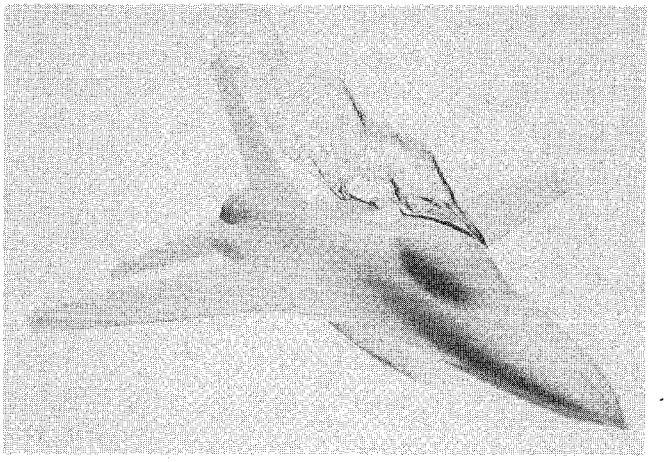

Fig. 12 Pitot pressure contours in a streamwise plane cut across the main wing and horizontal stabilizer at midspan.

fuselage/strake produced 48% of the lift and 62% of the drag with the wing producing 51% of the lift and 33% of the drag.

Flowfield Features

In Fig. 10, pitot pressure contours at a few selected streamwise stations present the vortical structure of the entire flowfield. The orderly development of the strake vortex is clearly discernible in this composite graph. This particular vortex system remains intact despite strong interactions with structures emanating from the wing and the vertical stabilizer. At this angle of attack, the vortex originating from the forebody gains strength as it proceeds over the canopy to finally merge with the strake vortex as it proceeds downstream. A secondary vortical structure on the fuselage can also be identified downstream of the wing-body juncture. Both horseshoe vortices generated by the tip of wing and the horizontal stabilizer remain separate entities in the wake. The wing-tip horseshoe vortex has been transported over a long distance to reach the display plane, and it is displaced farther away from the axis of the aircraft by the upwash.

The simulated surface oil pattern of Fig. 11 shows the footprint of these vortical structures. This surface shear pattern is generated by tracing the velocity components parallel and immediately adjacent to the aircraft contour. Unfortunately, there is no corresponding surface oil film record from the comparing data base to verify the present result.[23] However, available test results with a different wing configuration suggest that these results exhibit only qualitative affinity. On the lee surface, the attachment line of the strake vortex can be easily identified on the forebody. The weaker vortex from the forebody, however, leaves no clearly recognizable footprint.

Figure 12 contains pitot pressure contours in a plane cut across the wing and the horizontal stabilizer at the midspan. The highly dissipative portion of the wing wake is carried well above the horizontal stabilizer by the upwash, thus minimizing interference effects. As noted in the discussion of Fig. 8, the computation overpredicted the compression on the top surface of the wing and underpredicted that on the top surface of the horizontal stabilizer. One may conclude from this new evidence that the trends are not the same because of the wake-induced incidence angle and the anhedral of the horizontal stabilizer.

Concluding Remarks

A numerical simulation of the F-16A configuration has been accomplished at a freestream Mach number of 0.85, a Reynolds number of 12.75 million, and an angle of attack of 16.04 deg. Close comparison of surface pressure distributions with wind tunnel data produced reasonable results, and the aircraft lift coefficient matched existing data to within experimental tolerances. Although most essential physical features

of the flowfield have been reproduced, localized disparities from data are significant on the leeward surface and lead to an 8% overprediction of the drag coefficient. The most serious numerical errors remain concentrated near the leading edge of the lifting surfaces.

The present investigation restresses the basic issues of geometric resolution and numerical efficiency. Moreover, it points out the necessity of choosing an appropriate grid topology for calculation of flows at high angle of attack. Since leading-edge separation scales with the leading-edge radius, the correct simulation of features downstream demand resolution of this geometry.

Acknowledgments

Support from the Kirtland Air Force Base Computer Center and NASA Ames Research Center are deeply appreciated. Continuous assistance from G. Howell of General Dynamics, Fort Worth Division, and members of the Computational Aerodynamics Group, Wright Research and Development Center, are also gratefully acknowledged.

References

[1]Shang, J. S., and Scherr, S. J., "Navier-Stokes Solution for a Complete Re-entry Configuration," *Journal of Aircraft*, Vol. 23, No. 12, 1986, pp. 881–888; also AIAA Paper 75-1509, July 1985.

[2]Huband, G. W., Rizzetta, D. P., and Shang, J. S., "Numerical Simulation of the Navier-Stokes Equations for an F-16A Configuration," *Journal of Aircraft*, Vol. 26, No. 7, 1989, pp. 634–640; also AIAA Paper 88-2507, June, 1988.

[3]Flores, J., and Chaderjian, J. M., "A Zonal Navier-Stokes Methodology for Flow Simulation About A Complete Aircraft," AIAA Paper 88-2508, June 1988.

[4]Jameson, A., Baker T. J., and Weatherill, N. P., "Calculation of Inviscid Transonic Flow Over a Complete Aircraft," AIAA Paper 86-0103, Jan. 1986.

[5]Peak, D. J., and Tobak, M., "Three-Dimensional Interactions and Vortical Flows with Emphasis on High Speeds," AGARD-AG-252, July 1980.

[6]Shang, J. S., "An Assessment of Numerical Solutions of the Compressible Navier-Stokes Equations," *Journal of Aircraft*, Vol. 22, No. 5, 1985, pp. 353–370.

[7]Newsome, R. W., and Kandil, O. A., "Vortical Flow Aerodynamics—Physical Aspects and Numerical Simulation," AIAA Paper 87-0205, Jan. 1987.

[8]Thomas, J. L., Walters, R. W., Reu, T., Ghaffari, F., Weston, R. P., and Luckring, J. M., "A Patched-Grid Algorithm For Complex Configurations Directed Towards the F/A-18 Aircraft," AIAA Paper 89-0121, Jan. 1989.

[9]Schiff, L. B., Cummings, R. M., Sorenson, R. L., and Rizk, Y. M., "Numerical Simulation of High-Incidence Flow Over the F-18 Fuselage Forebody," AIAA Paper 89-0339, Jan. 1989.

[10]Ericsson, L. E., and Redding, J. P., "Aerodynamic Effects of Asymmetric Vortex Shedding From Slender Bodies," AIAA Paper 85-1797, Aug. 1985.

[11]Escudier, M. P., and Keller, J. J., "Vortex Breakdown: A Two State Transition," Aerodynamics of Vortical Flow in Three Dimensions, AGARD CP No. 342, April 1983, Paper No. 25.

[12]Leibovich, S., "Vortex Stability and Breakdown: Survey and Extension," *AIAA Journal*, Vol. 22, No. 9, 1984, pp. 1192–1206.

[13]Erisson, L. E., "The Fluid Mechanics of Slender Wing Rock," *Journal of Aircraft*, Vol. 21, No. 5, 1983, pp. 322–328.

[14]Rizzetta, D. P., and Shang, J. S., "Numerical Simulation of Leading-Edge Vortex Flows," *AIAA Journal*, Vol. 24, No. 2, 1986, pp. 237–245.

[15]Thomas, J. L., and Newsome, R. W., "Navier-Stokes Computations of Lee-Side Flows Over Delta Wings," AIAA Paper 86-1049, May 1986.

[16]Murman, E. M., Powell, K. G., Miller, D. S., and Wood, R. M., "Comparison of Computational and Experimental Data for Leading Edge Vortex Effects of Yaw and Vortex Flaps," AIAA Paper 86-0439, Jan. 1986.

[17]Fujii, K., and Schiff, L. B., "Numerical Simulation of Vortical Flows over a Strake-Delta Wing," *AIAA Journal*, Vol. 27, No. 9, 1989, pp. 1153–1162.

[18]Webster, W. P., and Shang, J. S., "Numerical Simulation of Reversed Flow over a Supersonic Delta Wing at High Angle of Attack," AIAA Paper 89-1802, Jan. 1989.

[19]Vadyak, J., and Schuster, D. M., "Navier-Stokes Simulation of Burst Vortex Flowfield for Fighter Aircraft at High Incidence," AIAA Paper 89-2190, Aug. 1989.

[20]MacCormack, R. W., "The Effect of Viscosity in Hypervelocity Impact Cratering," AIAA Paper 69-354, April 1969.

[21]Baldwin, B. S., and Lomax, H., "Thin-layer Approximation and Algebraic Model for Separated Turbulent Flows," AIAA Paper 78-0257, Jan. 1978.

[22]Shang, J. S., Hankey, W. L., and Petty, J. S., "Three-dimensional Supersonic Interacting Turbulent Flow Along a Corner," *AIAA Journal*, Vol. 17, No. 7, 1979, pp. 706–713.

[23]Reue, G. L., Doverenz, M. E., and Wilkins, D. D., "Component Aerodynamic Load from 1/9-scale F-16A Loads Model," General Dynamics Report, Fort Worth, TX, 16PR316, May 1976.

[24]Karman, S. L., Steinbrenner, J. P., and Kisielewski, K. M., "Analysis of the F-16 Flow Field by a Block Grid Euler Approach," AGARD Conference Proceedings No. 412, November 1986, pp. 18.1–18.8.

[25]Gustafasson, B., and Sandstrom, A., "Incompletely Parabolic Problems in Fluid Dynamics," *Journal of Applied Mathematics*, Vol. 35, No. 2, 1978, pp. 343–357.

[26]Engquist, B., and Majda, A., "Absorbing Boundary Conditions for the Numerical Simulation of Waves," *Mathematics of Computation*, Vol. 31, No. 139, 1977, pp. 629–651.

[27]Jameson, A., "A Non-Oscillatory Shock Capturing Scheme Using Flux Limited Dissipation," Dept. of Mechanics and Aerospace Engineering, Princeton University, Princeton, NJ, Report 1653, 1984.